Antarctic Science 2 (1): 29–42 (1990)

A one-dimensional mixed layer model beneath the Ross Ice Shelf with tidally induced vertical mixing

M. SCHEDUIKAT and D.J. OLBERS

Alfred-Wegener-Institut für Polar- und Meeresforschung, Postfach 120161, Columbusstraße, 2850 Bremerhaven, Federal Republic of Germany

Abstract: The dense High Salinity Shelf Water (HSSW) which spreads out below parts of the Ross Ice Shelf represents a heat-reservoir that can induce ablation if it comes into contact with the ice shelf base. One source of the mechanical energy necessary to lift the dense HSSW is small-scale turbulence induced by the shear of tidal currents at the sea-floor and at the ice shelf base. A one-dimensional Kraus-Turner-type model which is forced by a barotropic tidal current is coupled to the ice shelf by postulating that the ice–water interface is at the freezing point. The calculations indicate that the results of this two-layer approach allow a classification into a freezing and melting regime, depending strongly on the variability of the tidal currents with time and less on the intensity and the corresponding high production rate of turbulent kinetic energy. Based on an extended three-layer model ablation rates exceeding 0.4 m yr^{-1} are obtained in the south-eastern part of the Ross Ice Shelf. Advection processes in the mixed layer directly beneath the ice shelf base are not considered. These results can therefore be regarded as indicating the maximum amount of ablation occuring in the deeper reaches of the ice shelf cavity. Application of the three-layer model to the J9-area in the central Ross Ice Shelf indicate a tidally induced vertical heat flux of 1.8 W m^{-2} and a corresponding melting rate of 0.17 m yr^{-1}. As supported by ice core measurements, however, an accumulation rate of 0.03–0.05 m yr^{-1} is estimated due to advection of freshwater produced immediately south of the J9-area.

Received 5 June 1989, accepted 1 December 1989

Key words: barotropic tide, bottom ablation, thermodynamic coupling.

Introduction

In the western part of the Ross Sea, and especially in winter, cold offshore and katabatic winds force sea ice formation. Rejection of salt increases the density of the upper layers of the ocean until convection takes place and the dense water is mixed down. The High Salinity Shelf Water (HSSW) is characterized by potential temperatures $\Theta \leq -1.8$°C and a salinity $S \geq 34.75$‰. According to Gill (1973) the HSSW is expected to be produced in the Ross Sea at a rate of at least 0.6×10^6 m^3 s^{-1}, and probably more by a factor ×2 or ×3.

Because of the bottom topography and its density the HSSW spreads out below the Ross Ice Shelf (RIS). At station J9 in the central RIS (82°22.5'S, 168°37.5'W) the lower water column consists of HSSW up to 500 m below sea level. This suggests that HSSW will be found in most areas beneath the RIS (MacAyeal 1984*a*). The *in situ* temperature of this dense water mass is about 0.2°C to 0.5°C higher than the freezing point at the ice shelf base. The dense HSSW thus represents a heat and salt-reservoir that can induce ablation if it comes into contact with the ice shelf.

Hydrographic profiles recorded at station J9 indicated that HSSW resides in the lower part of the water column; it is a 35 m to 40 m thick layer with a homogeneous temperature distribution. This well-mixed layer is separated by an intermediate layer with a near-constant temperature gradient from a boundary layer directly beneath the ice shelf. This upper mixed layer is characterized by temperatures in the range of –2.13°C to –2.16°C which is close to the freezing point of sea-water at this depth (Gilmour 1979, Foster 1983). Jacobs *et al.* (1979) detected freezing conditions (T = –2.16°C, S = 34.39‰) near the ice–sea-water interface.

The vertical heat flux necessary to enable melting at the ice shelf base would be induced by raising the dense warm HSSW. This, however, requires mechanical energy. The ocean in the sub-ice-shelf cavity is isolated from direct interaction with the atmosphere. Therefore the tidal currents are the only likely mechanism to destroy the stratification (MacAyeal 1984*a*). Current-measurements at station J9 carried out by Jacobs *et al.* (1979) recorded velocities up to 0.17 m s^{-1} in a record of 6 hour length and found evidence that the main current component results from tidal oscillations.

Numerical simulations carried out by MacAyeal (1984*b*) showed that the main tide below the RIS, the barotropic diurnal K_1-tide, attains velocities up to 0.4 m s^{-1}, especially in regions where the ice shelf runs aground. Small scale turbulence produced by shear of tidal currents at the ice shelf base and at the sea-floor enables the development of well-mixed boundary layers. Associated entrainment processes would then cause an upward heat flux which produces melting at the ice shelf base. MacAyeal (1984*a*, 1985*b*) indicated that these processes may cause a deep thermohaline circulation in the sub-ice-shelf cavity which is characterized by inflow of dense HSSW in the lower part of the water

https://doi.org/10.1017/S0954102090000049 Published online by Cambridge University Press

column and outflow of buoyant melt-water plumes along the sloping ice shelf base. This circulation scenario is opposite to that proposed by Zotikov (1986) and Zotikov *et al.* (1980) who expected inflow just beneath the ice shelf base of low salinity water with temperatures 0.2°C–0.3°C above the *in situ* freezing temperature at the ice–sea-water interface. This would result in high ablation rates nearest to the ice shelf front and freezing in the central regions of the ice shelf and near the grounding line. However, MacAyeal (1985*b*) provided evidence that the modification of a melt-water plume moving from the deeper reaches of the ice shelf cavity to the ice shelf front may result in the formation of Deep Ice Shelf Water (DISW), depending on the intensity of the entrainment process and the corresponding ablation rates. DISW is found along the central and western part of the RIS-front at intermediate depth (Jacobs *et al.* 1970, 1979) and displays characteristics of pure glacial melt-water and HSSW (Jacobs *et al.* 1985).

Due to the importance of the vertical mixing process for the formation of water masses beneath the ice shelf it is necessary to give quantitative estimates of the local entrainment, ablation and accumulation rates. The tidally induced vertical mixing processes are therefore parameterized in a one-dimensional mixed layer model of integral type (Kraus & Turner 1967) which is coupled thermodynamically to the ice shelf. The first attempt is a simple model describing a two-layered ocean: a turbulent boundary layer directly beneath the ice shelf above a laminar bottom layer with fixed temperature and salinity. In this approach the bottom layer plays the role of an infinitely large heat and salt-reservoir. The model is forced by a tidal current assumed to be barotropic.

One question to be answered with the help of this simple approach is whether tidal currents generate enough small-scale turbulence at the ice shelf base to lift up dense bottom water and to create the observed thickness of the homogeneous layer directly beneath the RIS. Another question is whether the ablation/accumulation rate depends on intensity and time variability of the tidal currents.

The second part of this study presents an extended model. Below the upper boundary layer an intermediate layer is added which allows for gradients in profiles of temperature and salinity. The lower layer, representing the heat and salt-reservoir, now is treated as a turbulent boundary layer as well. In addition advection of warm and salty water in the bottom mixed layer is included. The three-layer model is applied to conditions at J9 in the central RIS in order to determine the vertical heat flux and the corresponding basal melting caused by tidal stirring. In addition ablation rates in the south-eastern part of the RIS, the expected origin of the DISW, are calculated based on the extended model. The calculations are restricted to regions of the RIS where the ice shelf draft exceeds 400 m which is the upper limit of the DISW mass on the Ross Sea continental shelf (Jacobs *et al.* 1970, 1979).

Description of the two-layer model

The basis of the two-layer model is the mixed layer model developed by Kraus & Turner (1967). The configuration of the model is shown in Fig. 1. The horizontally homogeneous mixed layer is covered by a floating ice shelf of thickness I. At the interface of atmosphere and ice a constant temperature T_A is prescribed. The temperature within the ice sheet is assumed to decrease linearly with depth to the freezing point at the ice–sea-water interface. This seems to be a sufficient approximation of real conditions (see: Clough & Hansen 1979, Jacobs *et al.* 1979). The freezing temperature T_1 is determined by the local salinity S_1 and pressure p. The freezing point condition is assumed to hold in an infinitely thin layer at $z = 0$ which consists of the lowest ice layer and the uppermost sea-water layer. The quasihomogeneous mixed layer has the mean temperature T_o, mean salinity S_o and thickness h_o. The bottom layer is held at constant temperature T_b and salinity S_b. The interfaces at $z = 0$ and $z = -h_o$ represent discontinuities in the stratification.

In the mixed layer (ML) horizontal homogeneity is assumed and molecular heat and salt fluxes as well as heat production due to viscous effects are neglected. Separating temperature and salinity in the Reynolds sense into time mean $\bar{T}$ and $\bar{S}$ and

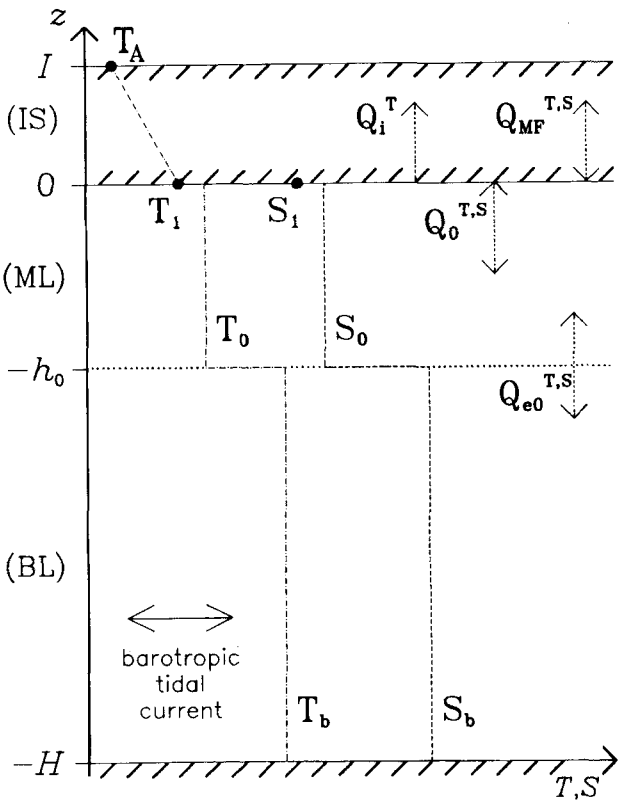


Fig. 1. Configuration of the two-layer model. Indicated are temperature and salinity profiles in the ice shelf (IS), the mixed layer (ML) and the bottom layer (BL) as well as the considered entrainment fluxes across discontinuity at $z = -h_o$ and the heat and salt fluxes at the base of the ice shelf.

https://doi.org/10.1017/S0954102090000049 Published online by Cambridge University Press

fluctuations T' and S' the conservation equations for heat and salt are

$$\frac{\partial \overline{T}}{\partial t} + \frac{\partial}{\partial z}\overline{w'T'} = 0 \quad (1)$$

$$\frac{\partial \overline{S}}{\partial t} + \frac{\partial}{\partial z}\overline{w'S'} = 0 \quad (2)$$

Here t is time, z is the vertical coordinate (z positive upwards), $\overline{w'T'}$ and $\overline{w'S'}$ are turbulent fluxes describing the correlation between the vertical component w' of the velocity fluctuation and the deviations T' and S' from the mean temperature and salinity field.

Equations (1) and (2) are coupled with the density field by the equation of state for sea-water. This equation reads in its linearized form:

$$\rho = \rho_r\{1 - \alpha(T - T_r) + \beta(S - S_r)\} \quad (3)$$

The subscript r denotes constant reference values of density, temperature and salinity. The coefficients α and β are the thermal and haline expansion of density ρ at reference values T_r and S_r and pressure p. The values used in the present calculations are: $T_r = -2.0°C$, $S_r = 35.0‰$, $p = 363$ dbar, $\alpha = 3.62 \times 10^{-5}\ °C^{-1}$, $\beta = 7.83 \times 10^{-4}\ ‰^{-1}$.

The postulated vertical homogeneity of the ML permits an integration of (1) and (2) from the upper limit of the turbulent layer at $z = 0$ to depth $z = -h_o$. This yields equations for the mean temperature and salinity

$$h_o \frac{d}{dt} T_o = -\overline{w'T'}\,|_{z=0} + \overline{w'T'}\,|_{z=-h_o} \quad (4)$$

$$h_o \frac{d}{dt} S_o = -\overline{w'S'}\,|_{z=0} + \overline{w'S'}\,|_{z=-h_o} \quad (5)$$

Turbulent heat and salt fluxes at the base of the ML are parameterized by differences of temperature and salinity between the turbulent layer and the laminar fluid below. The velocity of the mixing process is described by the entrainment velocity w_{eo} (Niiler & Kraus 1977). This yields

$$\overline{w'T'}\,|_{z=-h_o} = w_{eo}(T_b - T_o) \quad (6)$$

$$\overline{w'S'}\,|_{z=-h_o} = w_{eo}(S_b - S_o) \quad (7)$$

The turbulent fluxes at $z = 0$ are assumed to be proportional to temperature andd salinity differences between the top of the ML and the ice–sea-water interface

$$\overline{w'T'}\,|_{z=0} = \gamma_T(T_o - T_1) \quad (8)$$

$$\overline{w'S'}\,|_{z=0} = \gamma_S(S_o - S_1) \quad (9)$$

with coefficients γ_T and γ_S which are characteristic velocities for the transfer of heat and salt across infinitesimal sublayers.

Laboratory experiments to determine the velocity distribution of turbulent flow in tubes with smooth and rough surfaces have indicated that the boundary layer is divided into three parts (McPhee *et al.* 1987, Schlichting 1982, p. 600):

a. A laminar sublayer dominated by viscous effects.
b. A transition zone (buffer layer) characterized by turbulent as well as viscous processes.
c. A fully turbulent layer where viscous effect are negligible.

McPhee *et al.* (1987) pointed out that even if the roughness Reynolds number is high, molecular heat and salt fluxes should be considered in order to predict melt rates. Otherwise the calculated rates become unrealistic. The characteristic velocities γ_T and γ_S are therefore determined by the molecular diffusion coefficients for heat and salt, κ_T and κ_S respectively, and by the thickness of thermal and haline sublayers.

Knowledge about the small scale roughness at the ice shelf base is poor. Zotikov *et al.* (1980) deduced from an ice core that in regions dominated by freezing of sea-water the roughness length scale is in the order of magnitude of 1 to 2 mm due to the structure of the accumulated ice crystals. In regions dominated by ablation processes the ice shelf base is assumed to be smooth. In this case the thickness of the viscous sublayer d can be estimated from (Schlichting 1982, p. 600):

$$d \approx 5\frac{\nu}{u_*} \quad (10)$$

Here $\nu = 1.95 \times 10^{-6}\ m^2\ s^{-1}$ is the kinematic viscosity of sea-water at temperatures just above the freezing point and $u_* = 5.0 \times 10^{-3}\ m\ s^{-1}$ is the friction velocity for typical tidal currents beneath the RIS (MacAyeal 1984*b*). This yields $d \approx 2$ mm.

Heat transfer within the laminar sublayer takes place under circumstances like those in fully laminar flow (Holman 1986, p. 225). In this instance the thickness of the thermal sublayer may be calculated from

$$d_T = \frac{d}{1.026} Pr^{-1/3} \quad (11)$$

The ratio $Pr = \nu/\kappa_T$ is called the Prandtl number; it relates the relative thickness of the hydrodynamic and thermal boundary layers. Equation (11) only holds for fluids with Prandtl Numbers greater than about 0.7 (Holman 1986, p. 226). With $\kappa_T = 1.35 \times 10^{-7} m^2\ s^{-1}$ this yields $d_T \approx 1$ mm. Thus, $\gamma_T = \kappa_T/d_T = 1.35 \times 10^{-4}\ m\ s^{-1}$. Assuming that the thickness of the haline sublayer d_S is equal to d_T the resulting characteristic velocity is $\gamma_S = \kappa_S / d_S = 6.8 \times 10^{-7}\ m\ s^{-1}$.

Inserting the specified fluxes (6) to (9) into (4) and (5) leads to prognostic equations:

$$\frac{d}{dt} T_o = \frac{1}{h_o}[w_{eo}(T_b - T_o) - \gamma_T(T_o - T_1)] \quad (12)$$

$$\frac{d}{dt} S_o = \frac{1}{h_o}[w_{eo}(S_b - S_o) - \gamma_S(S_o - S_1)] \quad (13)$$

Evolution of the ML-thickness with time can be described with the help of the entrainment velocity w_{eo} (Niiler & Kraus 1977).

$$\frac{d}{dt} h_o = w_{eo}; \qquad w_{eo} > 0 \quad (14)$$

This prediction equation is not used if the turbulent kinetic energy budget gets negative. Then h_o is calculated diagnostically from $w_{eo}(h_o) = 0$. The above formulation

https://doi.org/10.1017/S0954102090000049 Published online by Cambridge University Press

expresses that the entrainment flux is always directed towards the fluid of higher turbulence, upwards in this case (Phillips 1977). If the available turbulent kinetic energy is not sufficient to maintain the thickness of the ML, the entrainment velocity w_{eo} becomes zero and the thickness will decrease (detrainment).

In order to close the system of equations (12) to (14) an expression for the entrainment velocity w_{eo} is needed. We are following the reasoning of Niiler & Kraus (1977) and will discuss the integrated balance equation for turbulent kinetic energy (TKE). Assuming a complete balance between production and dissipation of TKE leads to

$$-\int_{-h_o}^{0}\overline{w'\underline{v}'}\;\frac{\partial}{\partial z}\overline{\underline{v}}dz-\int_{-h_o}^{0}\frac{\partial}{\partial z}\left[\overline{w'\left(\frac{p'}{\rho}+\frac{E}{2}\right)}\right]dz \qquad (15)$$
$$+\int_{-h_o}^{0}\overline{w'b'}dz-\int_{-h_o}^{0}\varepsilon\,dz=0$$

Here $\overline{\underline{v}}$ and $\underline{v}'$ are the mean and fluctuating part of the horizontal velocity $\underline{v}=(u,v)$, E is the sum of the squares of the turbulent velocity components; $E=u'^2+v'^2+w'^2$, b' is the fluctuating part of the buoyancy $b=-g(\rho-\rho_r)/\rho_r$ and ε is the viscous dissipation of TKE. The first term on the left hand side represents shear production of TKE, the second term is the transport (self diffusion) by vertical velocity fluctuations of TKE and pressure fluctuations p'. The third term describes the work done by turbulence against buoyancy forces and the accompanied change of potential energy of the system. Notice that $\overline{w'b'}=g(\alpha\,\overline{w'T'}-\beta\,\overline{w'S'})$. The last term stands for conversion of TKE into thermal energy due to molecular friction and will be assumed to be proportional to the ML-depth and TKE-producing processes. In order to get an expression for w_{eo} adequate parameterizations for the turbulence producing and consuming components at $z=0$ and $z=-h_o$ must be found.

The model is forced by a barotropic tidal current. The net shear production of the flow at the ice shelf base (no slip boundary condition) is assumed to be of the form

$$-\int_{-h_o}^{0}\overline{w'\underline{v}'}\;\frac{\partial}{\partial z}\overline{\underline{v}}dz-\int_{-h_o}^{0}\varepsilon_s dz=D_o\exp\left(\frac{-h_o}{h_s}\right)u_*^3 \qquad (16)$$

where ε_s is the dissipation in respect to the shear production and u_* is the friction velocity at the ice shelf base defined by $u_*=(C\,|\underline{v}|^2)^{1/2}$. The drag coefficient C is taken to be 2.5×10^{-3} (from MacAyeal 1984*b*) and $|\underline{v}|=(u^2+v^2)^{1/2}$ is the absolute value of the velocity vector $\underline{v}$ with components $u=U_o\cos\omega t$ and $v=V_o\sin\omega t$ of the tidal current ellipse. The dissipation length scale is taken to be $h_s=7$ m, following Lemke & Manley (1984), and the constant factor is choosen to be $D_o=6$ for standard calculations.

Assuming that the turbulent buoyancy flux, $\overline{w'b'}$ decreases linearly with depth the change of potential energy of the ML is

$$-\int_{-h_o}^{0}\overline{w'b'}dz-\int_{-h_o}^{0}\varepsilon_c\,dz=\frac{1}{2}D_c\,h_o\,B_o-\frac{1}{2}w_{eo}h_o\,\Delta B \qquad (17)$$

Here ε_c stands for the dissipation in respect to the production of TKE due to buoyancy effects. The first term on the right hand side describes the contribution of the surface flux ($B_o\equiv g[\alpha\,\overline{w'T'}|_{z=0}-\beta\,\overline{w'S'}|_{z=0}]$). A parameter D_c is introduced which determines the net contribution of the produced convective turbulence to the TKE budget.

$$D_c\exp\left(\frac{-h_o}{h_c}\right);\qquad B_o>0 \qquad (18)$$
$$D_c=1;\qquad B_o<0$$

In the present case convective turbulence is produced only if cooling or a salinity-increase takes place at the top of the ML ($B_o>0$). The dissipation length scale h_c is taken to be 50 m following Lemke & Manley (1984). The second term on the right hand side of (17) represents the reduction of potential energy by lifting of the dense entrained water, where $\Delta B=g[\alpha(T_o-T_b)-\beta(S_o-S_b)]$.

At $z=0$ self diffusion of TKE makes no contribution to the balance. The portion at $z=-h_o$ describes the amount of turbulence energy per unit area and time which must be supplied by the downward flux to make the entrained (laminar) water as agitated as the ML-water. We will neglect this term in comparison to the remaining terms (Niiler & Kraus 1977).

In order to prevent the ML-depth h_o becoming infinite (if $B_o>0$) we will follow Niiler (1975) and introduce a background dissipation which is assumed to be proportional to the depth of the ML.

$$\int_{-h_o}^{0}(\varepsilon-\varepsilon_s-\varepsilon_c)dz=\varepsilon_o h_o \qquad (19)$$

Inserting (16), (17) and (19) into (15) and solving for w_{eo} leads to

$$w_{eo}=\frac{2D_o\exp(-h_o/h_s)u_*^3+D_c\,h_o\,B_o-2\varepsilon_o h_o}{\Delta B\,h_o} \qquad (20)$$

Now h_o can be calculated from (14) when there is enough TKE available to deepen the ML.

The freezing point T_1 at the ice–sea-water interface and the corresponding salinity S_1 follow from the balances of heat and salt fluxes at the ice shelf base. The heat balance is written in terms of the heat loss due to molecular heat conduction into the ice, the latent heat flux and the turbulent flux.

$$\rho_i c_i \kappa_i\frac{T_A-T_1}{l}-\rho_i w_i L+\rho_W c_p \gamma_T(T_o-T_1)=0 \qquad (21)$$

Here ρ_i is the density of the ice shelf (taken to be 916.4 kg m^{-3}), c_i is the specific heat capacity of ice ($c_i=2.094\times10^3$ J $°C^{-1}$ kg^{-1}), κ_i is the thermal diffusivity in the ice ($\kappa_i=1.156\times10^{-6}$ m^2 s^{-1}), w_i the melting rate ($w_i>0$ for ablation). $L=3.336\times10^5$ J kg^{-1} is the latent heat of fusion and $c_p=3.98\times10^3$ J $°C^{-1}$ kg the specific heat of sea-water at constant pressure. In analogy the salt balance reads

$$\rho_W\gamma_S(S_o-S_1)-\rho_i w_i S_1=0 \qquad (22)$$

Molecular salt fluxes into the ice are neglected in comparison

https://doi.org/10.1017/S0954102090000049 Published online by Cambridge University Press

to other fluxes. To get expressions for T_1, S_1 and w_i a third equation is needed. This is the freezing point condition at the ice shelf base which is taken here in a linearized form

$$T_1 = aS_1 + b \tag{23}$$

where a is the gradient $(\partial T_f/\partial S)$ of the freezing point of seawater (Gill 1983, p. 602) at salinity S_{ref} and b is given by

$$b = T_{ref} - aS_{ref} \tag{24}$$

where T_{ref} stands for the freezing point at S_{ref} and pressure p. Solving (21) to (23) for the melting rate yields

$$w_i = \frac{a\,\rho_W \gamma_T \gamma_S c_p (T_o - T^*) - A\,\gamma_S (T_A - T_1)}{\rho_i(\gamma_S L - a\,c_p\,\gamma_T S_1)} \tag{25}$$

where $A = \rho_i c_i k_i / l$ and $T^* = aS_o + b$ is the freezing point corresponding to the ML-salinity S_o. For the temperature at the interface we find

$$T_1^{(a,b)} = -\frac{k}{2} \mp \sqrt{\frac{k^2}{4} - l} \tag{26}$$

where

$$k = -\left[\frac{AT_A + \rho_W \gamma_S L + \rho_W \gamma_S c_p T_o + \rho_W \gamma_T c_p b + Ab}{A + \rho_W c_p \gamma_T}\right]$$

$$l = \left[\frac{\rho_W \gamma_S L T^* + A T_A b + \rho_W T_o \gamma_T + c_p b}{A + \rho_W c_p \gamma_T}\right]$$

Solution $T_1^{(b)}$ is inconsistent with the freezing point condition (23) which is only valid for $S_1 \geq 0$. For S_1 we get from (23)

$$S_1 = \frac{T_1^{(a)} - b}{a} \tag{27}$$

The three diagnostic equations (25) to (27) as well as the equations (12) to (14) and (20) represent a closed system in order to solve for T_1, S_1, w_i, T_o, S_o, h_o and w_{eo}.

Results of the two-layer model

Intensity and time variability of the TKE-source (16) depend on magnitude and ratio of the axes U_o and V_o of the tidal current ellipse. Based on numerical results of MacAyeal (1984*b*) the model forcing was varied. Results for $\bar{h}_o$ and $\bar{w}_i$ (mean over the period $\tau = 23.9\,h$ of the K_1-tide) are sketched in Figs 2 and 3. There is a strong dependence of the melting rate on the shape of the tidal ellipse, allowing a classification of the results into an ablation and an accumulation regime.

If the tidal current is isotropic ($U_o = V_o$) the forcing is constant in time. In this case the system assumes a steady state characterized by a freezing rate of 1.3 cm yr^{-1}, independent on the intensity of the forcing, and a ML-depth ranging from 8 m to 44 m, depending on the velocity of the tidal current. During the development of the ML warm and salty water is entrained from below. The ML is warmed up and a distinct portion of the gained heat is used to melt the ice shelf. In spite of further steady forcing the net production of TKE decreases due to the linear increase of the background dissipation with

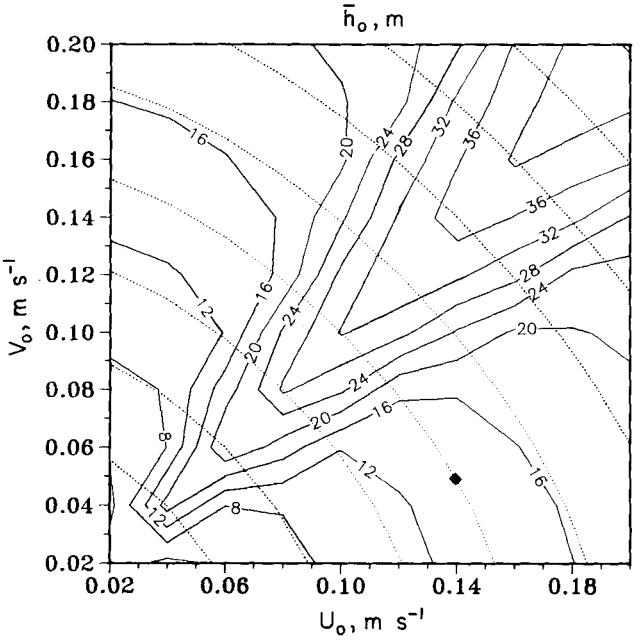


Fig. 2. Mixed layer thickness $\bar{h}_o$ (mean over a tidal cycle) in dependence on the magnitude of the axis U_o and V_o of the tidal current ellipse. The dotted lines connect points characterized by equivalent mean friction velocity $u_*(t)$. The results for the indicated combination of U_o and V_o (forcing for the anisotropic standard run) are described in detail in the text.

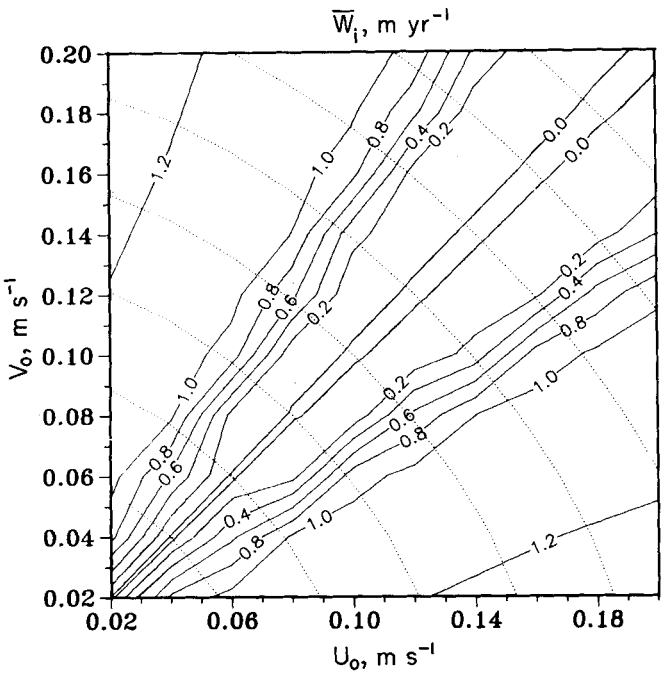


Fig. 3. Dependence of the melting/freezing rate $\bar{w}_i$ on the vector components of the tidal current ellipse. Around the axis of symmetry $(U_o = V_o)$ $\bar{w}_i < 0$. The minimum is $\bar{w}_i = -1.3$ cm yr^{-1}.

https://doi.org/10.1017/S0954102090000049 Published online by Cambridge University Press

h_o. Proceeding in time the entrainment velocity w_∞ converges to zero. The heat loss at the top of the ML will therefore exceed the heat gain due to the entrainment heat flux, and as a result the ML cools down to T_1. At steady state the balance of the heat fluxes at the ice–sea-water interface (21) is determined by the heat loss due to molecular heat conduction into the ice shelf and the latent heat flux. Despite the net positive contribution of the buoyancy effect ($B_o > 0$) the main balance in (15) is determined by the net shear production rate and dissipation in the background.

Forcing the system with anisotropic tidal currents a cyclic state is produced with melting rates up to 1.4 m yr^{-1} (Fig. 3). Results for $U_o = 0.14$ m s^{-1} and $V_o = 0.05$ m s^{-1} indicated by a square in Fig. 3 are shown in Figs 4 and 5.

The tidal cycle is marked by alternating entrainment and detrainment conditons. Because of the symmetry of the tidal current ellipse the cycle has a period $\tau_c \approx \tau/2$. The forcing has its maximum at phase angles $\varphi = 0°$ and $\varphi = 180°$, the minimum is found at $\varphi = 90°$ and $\varphi \approx 270°$, respectively. During an entrainment situation warm and salty water is integrated in the ML. Thus, temperature T_o and salinity S_o are increasing because the entrainment fluxes are more intensive than the turbulent fluxes at the top of the ML. The ML-temperature lies above its freezing point T^*. Thus, the surplus of heat is used to melt the ice. TKE is needed in order to overcome the resulting buoyancy forces. The available TKE to enable a further development of the ML therefore tends to decrease. Proceeding in time the forcing and the net shear production decreases.

At $\varphi \approx 30°$ the state of the system changes to detrainment. Now the net production rate due to shear of the tidal current at the ice shelf base is no longer sufficient to balance buoyancy effects ($B_o < 0$). In contrast to the steady forced case dissipation of TKE in the background plays a minor role and can be neglected in this context. During the detrainment situation the retreat of the ML can be described by

$$h_o^* = \frac{2D_o \exp(-h_o^*/h_s)u_*^3}{|B_o|} \tag{28}$$

which yields the Monin-Obukhov length h_o^* of this model (Niiler & Kraus 1977). Thermodynamically the ML is decoupled from the lower layer. Only the heat and salt fluxes at the upper limit of the ML are still active. Thus, T_o and S_o are decreasing continuously over the period of detrainment. Former cold and low salinity ML-water left in the bottom layer is assumed to achieve the characteristics of the lower water mass immediately. This is equivalent postulating an advection of heat and salt with infinite velocity in the laminar bottom layer. The ML-water comes closer to its freezing point T^* because of cooling and freshening during the detrainment situation. The ablation rate decreases ($30° < \varphi < 90°$) but still has a relatively high value despite of missing entrainment fluxes. This is due to the ability of the ML to store heat and salt caused by the proposed parameterization of the turbulent fluxes at $z = 0$ proportional to characteristic velocities γ_T and γ_S which is limiting the upward heat and salt flux. This behaviour has to be taken into account in order to simulate processes having the time scales considered. Treating processes having significantly larger time scales it is sufficient to assume the ML to be at freezing point T^* (Lemke 1987).

After the forcing has passed its minimum at $\varphi = 90°$ the system switches to entrainment. Now the net production of TKE by shear is sufficient to overcome the buoyancy forces and to deepen the ML. At the onset of entrainment the corresponding fluxes are too weak to compensate the losses at the top of the ML. Therefore T_o and S_o are still decreasing as well as w_i. The period of time $90° < \varphi < 110°$ corresponds to a near-constant 'heat content' $W_T \approx h_o T_o$ and salt content $W_S = h_o S_o$ of the ML (Fig. 5a, b). After this the entrainment velocity is rising strongly and the ML deepens further. This results in an increasing heat content until the next detrainment

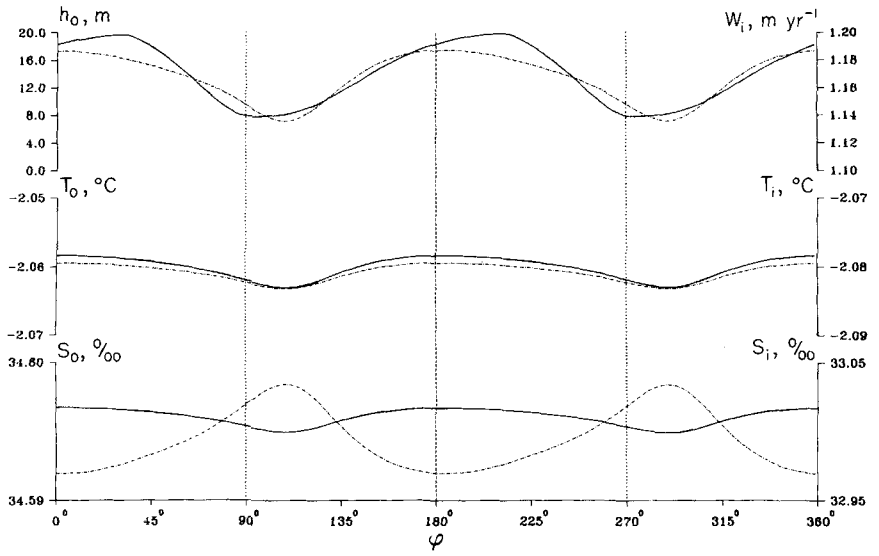


Fig. 4. Time series of the model variables for a prescribed anisotropic tidal current ($U_o = 0.14$ m s^{-1}, $V_o = 0.05$ m s^{-1}). The dashed curves belong to the ordinates on the right hand side.

https://doi.org/10.1017/S0954102090000049 Published online by Cambridge University Press

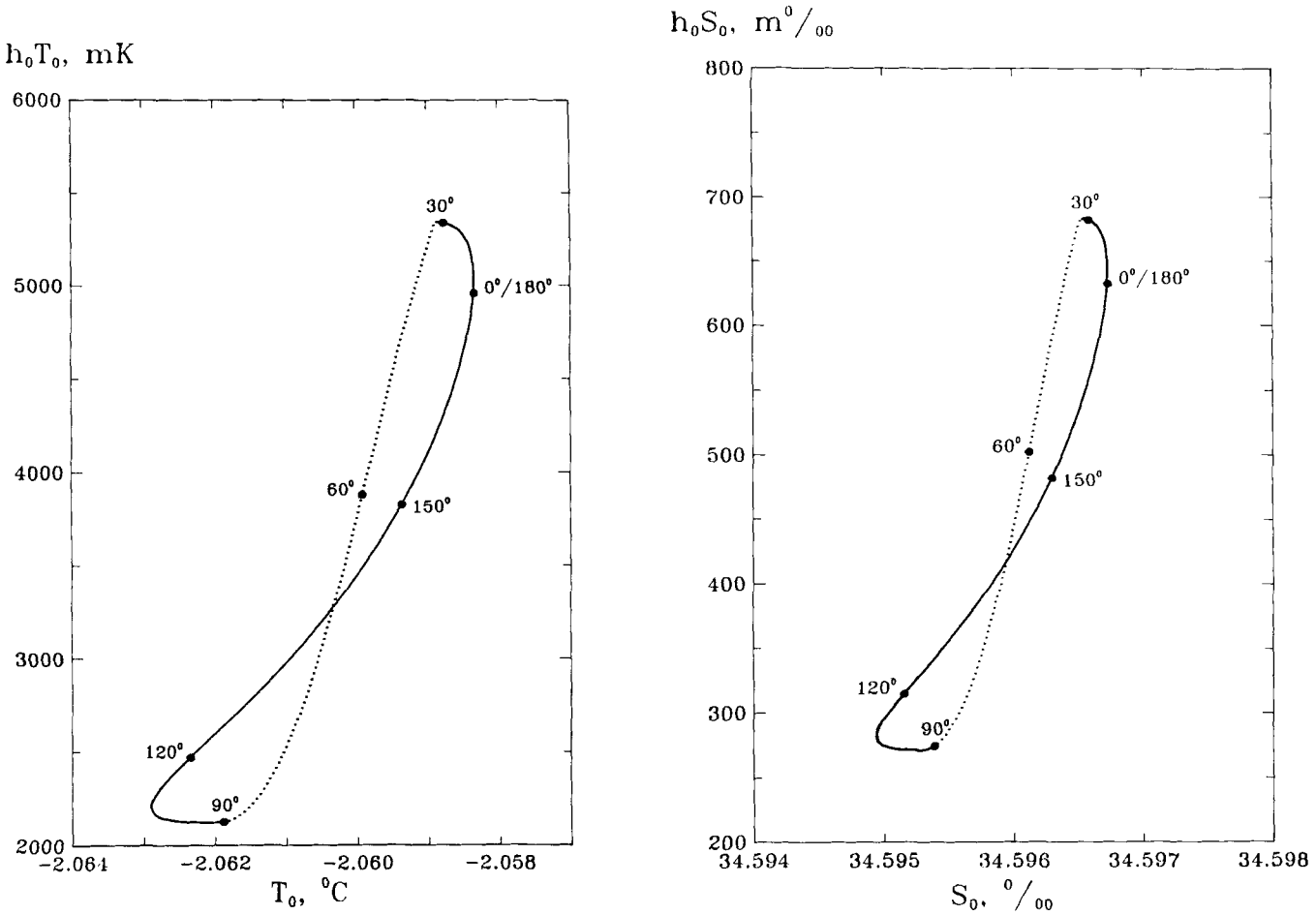


Fig. 5. Cycles of 'heat content' h_oT_o and temperature T_o (a) and of salt content h_oS_o and salinity S_o (b) during the tidal cycle. Dotted parts of the cycles indicate detrainment.

situation begins ($\varphi = 220°$) and the cycle starts again.

The higher the time variability of the tidal currents the stronger the alternating entrainment situations. The consequences are increasing melting rates and a corresponding decrease of the mean ML-thickness. The experiments described above indicate that the achieved model state (freezing or melting) is strongly determined by the variability with time of TKE and not by the intensity of the tidal current and the corresponding high production rate of TKE.

In addition sensitivity studies revealed that the modification of the parameters D_o, h_s, h_o, γ_T, γ_S has almost no influence on whether the model state will belong to the ablation or accumulation regime but has an effect on several other model quantities. At first we will consider the special case characterized by steady forcing. The parameter study shows a remarkable result. The rate of freezing remains invariable with regard to the modification of the parameters listed above. The accumulation is determined solely by the heat loss due to molecular heat conduction into the ice shelf. The explanation for this behaviour is the convergent development of the ML-depth. Whatever the resulting depth, the layer will achieve temperature T_1 at the ice shelf base because of missing entrainment fluxes. A modification of γ_T and γ_S only modifies the time scale the system will reach its final steady state. The model reacts most sensitively to the choice of D_o and the dissipation length scale h_s because the barotropic current is the only external forcing (Fig. 6). The bounds of D_o are chosen arbitrarily, the upper limit for h_s follows a parameterization used by J. Schröter (personal communication, 1988) in order to fit a ML-model to the observed temperature field in the northern Atlantic. The ML-depth could exceed 160.0 m (Fig. 6) which surely is unrealistic beneath an ice shelf. As indicated in Fig. 6 the calculations using the standard parameterizations yield realistic ML-depths.

If the forcing is variable with time the model is extremely sensitively to the choice of the characteristic velocities γ_T and γ_S. For increasing velocities very high ablation rates and corresponding low ML-depths occur (Fig. 7). The reason for this behaviour is the reduced ability of the ML to store heat and salt. The heat loss at the top of the ML increases linearly with γ_T. A larger portion of the entrained heat is therefore used to melt the ice immediately. Due to the amount of melt-

https://doi.org/10.1017/S0954102090000049 Published online by Cambridge University Press

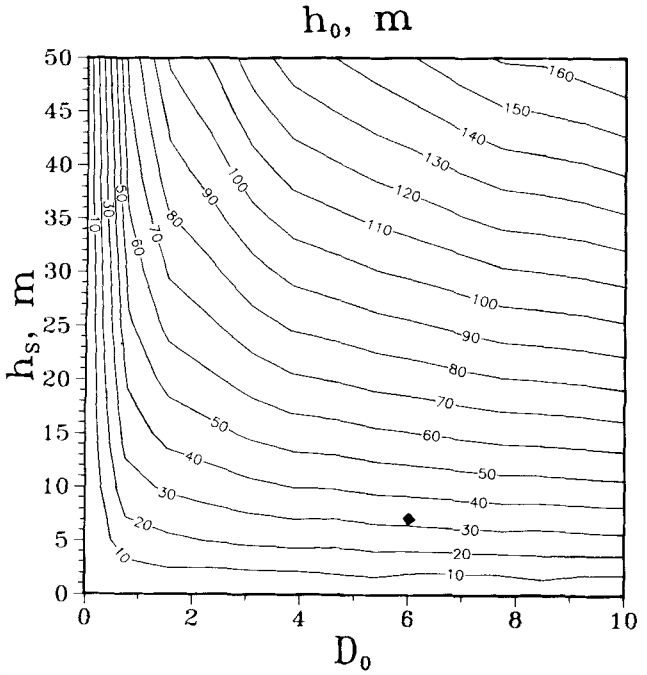


Fig. 6. ML-thickness h_o in dependence on parameter D_o and dissipation length scale h_s if constant forcing ($U_o = V_o = 0.10$ m s^{-1}) is prescribed. The square is indicating the combination of D_o and h_s used for standard calculations.

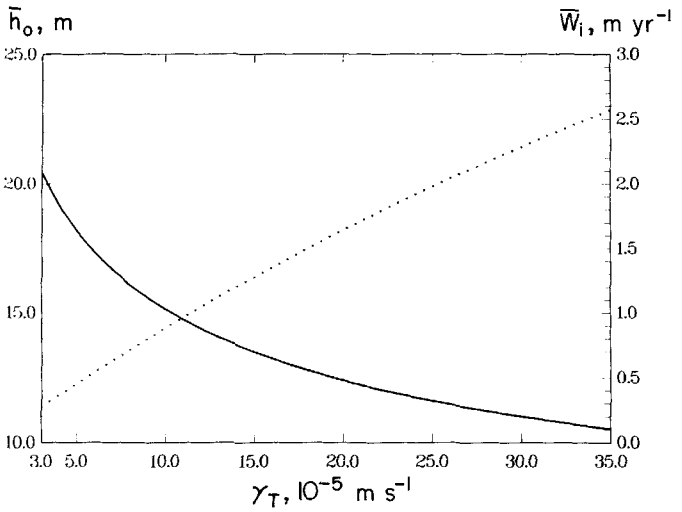


Fig. 7. Dependence of mean ML-thickness $\bar{h}_o$ and ablation rate $\bar{w}_i$ on characteristic velocity γ_T. The dashed curve belongs to the ordinate on the right hand side.

water produced the mean ML-depth decreases. Consequently entrainment fluxes become more efficient because the same amount of heat is mixed into a thinner water column. This additionally amplifies the rate of melting. Noticeable is the near-linear dependence of $\bar{w}_i$ on γ_T. This points to the fact that the differences of temperature and salinity between ML and the ice–sea-water interface are nearly constant but adjust at a lower level proportional to the characteristic velocities.

In comparison for the freezing regime the parameters D_o and h_s modify the results in a less extreme way. An increase of the dissipation length scale h_s results in a more efficient entrainment flux — so that the ratio of the thickness of the entrained water layer from below to the mean ML-thickness h_o increases. Consequently the rate of melting rises but does not exceed 1.4 m within the considered parameter bounds. The maximum mean ML-depth obtained amounts to 52.0 m and h_o is limited by the TKE-consuming buoyancy force which is proportional to w_i and h_o (see equation (17)).

Ablation rates calculated on the basis of the two-layer model are too high without exception. This is due to the character of the laminar bottom layer. We have assumed that this layer represents an infinite large heat and salt source which, however, is unrealistic. Consequently the calculated entrainment fluxes are overestimated.

Description of the three-layer model

To yield a better estimate for entrainment heat and salt fluxes at the base of the upper ML an extended model version has been developed. Taking into account the vertical structure of the stratification at station J9 in the central RIS an intermediate layer is included which separates the upper boundary layer and the bottom layer. The bottom layer now is treated as a turbulent boundary layer as well (Fig. 8) and an advective transport of heat and salt ($Q_{Adv}^{T,S}$) is included. The conservation equations for heat and salt in the bottom boundary layer in its integrated form then read

$$h_b \frac{d}{dt} T_b + \frac{1}{\rho_W c_p} Q_{Adv}^T = -\overline{w'T'}\,|_{z=-h_o-h_M} + \overline{w'T'}\,|_{z=-H} \tag{29}$$

$$h_b \frac{d}{dt} S_b + \frac{1}{\rho_W} Q_{Adv}^S = -\overline{w'S'}\,|_{z=-h_o-h_M} + \overline{w'S'}\,|_{z=-H} \tag{30}$$

where

$$\overline{w'T'}\,|_{z=-h_o-h_M} = w_{eb}(T_b - T_b^*) \tag{31}$$

$$\overline{w'S'}\,|_{z=-h_o-h_M} = w_{eb}(S_b - S_b^*) \tag{32}$$

Here T_b^* and S_b^* are the depth-averaged temperature and salinity in an entrainment zone of thickness δ (Lemke 1987). The thickness δ is defined by the diameter of typical turbulence elements which are entrained into the ML. The corresponding fluxes at the lower boundary at $z = -H$ are

$$\rho_w c_p \overline{w'T'}\,|_{z=-H} = Q_{Geo}^T \tag{33}$$

$$\rho_w w'S'\,|_{z=-H} = 0 \tag{34}$$

The geothermal heat flux through the seabed below RIS amounts to 54 mW m^{-2} (Foster 1978) and will be neglected in comparison to the advection of heat. Horizontal transfer of heat and salt is modelled by

$$\frac{1}{\rho_w c_p h_b} Q_{Adv}^T = u_a \frac{T_b - T_\infty}{L_\infty} \tag{35}$$

$$\frac{1}{\rho_w h_b} Q_{Adv}^S = u_a \frac{S_b - S_\infty}{L_\infty} \tag{36}$$

https://doi.org/10.1017/S0954102090000049 Published online by Cambridge University Press

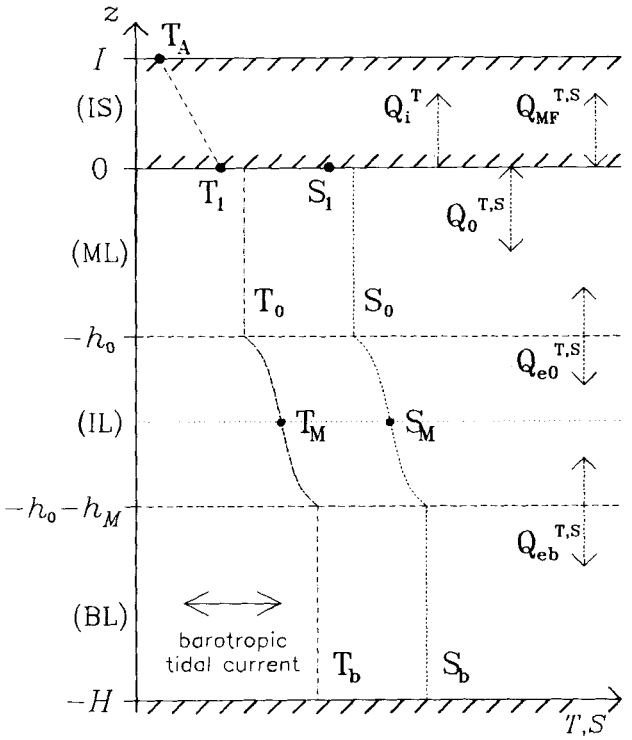


Fig. 8. Configuration of the three-layer model. Indicated are temperature and salinity profiles in the ice shelf (IS), the upper mixed layer (ML), the intermediate layer (IL) and the bottom boundary layer (BL) as well as the considered entrainment fluxes across the discontinuities at $z = h_o$ and $z = h_o - h_M$ and the heat and salt fluxes at the base of the ice shelf.

where T_∞ and S_∞ are temperature and salinity of a characteristic watermass (HSSW), L_∞ is the distance between this water mass and the location of interest and u_a represents the advection velocity. With regard to a hydrographic profile taken in the expected origin of HSSW north of Ross Island (Jacobs *et al.* 1979) the values for temperature and salinity used in the present calculation are $T_\infty = -1.84°C, S_\infty = 34.84‰$.

For the advection velocity we adopt an estimate of MacAyeal (1984*a*). Based on a channel model MacAyeal (1984*a*) estimated the velocity of the thermohaline circulation beneath the RIS to be in the order of $u_a = 0.01$ m s^{-1} which is consistent with the radioactive tracer measurements of Michel *et al.* (1979). A second process responsible for a steady barotropic circulation with magnitudes of the same order is the tidal rectification which, however, is rescricted to the ice shelf area closest to the ice front (MacAyeal 1985*a*) and therefore is outside the scope of this study. This yields the prognostic equations

$$\frac{d}{dt}T_b + u_a\frac{T_b - T_\infty}{L_\infty} = w_{eb}\frac{T_b^* - T_b}{h_b} \tag{37}$$

$$\frac{d}{dt}S_b + u_a\frac{S_b - S_\infty}{L_\infty} = w_{eb}\frac{S_b^* - S_b}{h_b} \tag{38}$$

For the lower ML we have in analogy to (14)

$$\frac{d}{dt}h_b = w_{eb}; \qquad w_{eb} > 0 \tag{39}$$

Following the same reasoning as before the expression for the entrainment velocity w_{eb} reads

$$w_{eb} = \frac{2D_o\exp(-h_o/h_s)u_*^3 - 2\varepsilon_o h_b}{\Delta B_b h_b} \tag{40}$$

where $\Delta B_b = g[\alpha(T_b^* - T_b) - \beta(S_b^* - S_b)]$. As stated above the ML-depth will be calculated diagnostically when the production of TKE is not sufficient for further deepening of the ML.

For the upper ML as well as for the conditions at the ice–sea-water interface the equations derived for the two-layer model are still valid. In equations (12) and (13), however, T_b and S_b have to be replaced by the averaged temperature T_o^* and salinity S_o^* in the entrainment zone, respectively.

The first step in order to derive expressions for T_o^*, S_o^*, T_b^* and S_b^* is to consider conservation equations for heat and salt content of the intermediate layer (IL). This transition-layer represents a passive element in the three-layer model. Its evolution is solely determined by the adjacent boundary layers. The conservation equations for the IL read

$$\frac{d}{dt}(h_M T_M) = G_T(w_{eo}) + G_T(w_{eb}) \tag{41}$$

$$\frac{d}{dt}(h_M S_M) = G_S(w_{eo}) + G_S(w_{eb}) \tag{42}$$

where h_M is the thickness and T_M, S_M are the vertical mean temperature and salinity of the IL. The function G_T is defined by

$$G_T(w_{eo}) = \begin{cases} -w_{eo}T_o^*; & w_{eo} > 0 \\ w_o T_o; & w_{eo} \equiv 0 \end{cases} \tag{43}$$

$$G_T(w_{eb}) = \begin{cases} -w_{eb}T_b^*; & w_{eb} > 0 \\ w_b T_b; & w_{eb} \equiv 0 \end{cases} \tag{44}$$

The function G_S is defined correspondingly. In (43) and (44) w_o and w_b describe the movement of the interfaces at $z = -h_o$ and $z = -h_o - h_M$ during a detrainment situation.

$$w_o = -\frac{d}{dt}h_o; \qquad w_{eo} \equiv 0 \tag{45}$$

$$w_b = -\frac{d}{dt}h_b; \qquad w_{eb} \equiv 0 \tag{46}$$

Taking into account (14) the thickness of the IL can be calculated during entrainment and detrainment periods of both the upper and lower ML using

$$h_M = H - h_o - h_b \tag{47}$$

where H represents the thickness of the water column beneath the ice shelf.

In principle the vertical mean temperature T_M and salinity S_M could be used in order to calculate the entrainment fluxes at discontinuities $z = -h_o$ and $z = -h_o - h_M$. Results of the two-layer model, however, suggested that this will overestimate these fluxes. The second step to yield expressions for T_o^*, S_o^*, T_b^* and S_b^* is to postulate the existence of structure functions $SF_{T,S}$ which describe the vertical distribution of T and S

https://doi.org/10.1017/S0954102090000049 Published online by Cambridge University Press

within the IL and allow for a difference between T_o^* and T_M as well as S_o^* and S_M. For simplicity only the equations for temperature are considered in the following. The equations for salinity can be derived correspondingly. The structure function $SF_T(z, T_o, T_b, T_M, h_M)$, has to be monotonic and continuous, though allowing for discontinuities in the gradients at $z = -h_o$ and $z = -h_o - h_M$. In addition SF_T has to comply with the condition

$$h_M T_M = \int_{-h_o-h_M}^{-h_o} SF_T(z, T_o, T_b, T_M, h_M)\, dz \tag{48}$$

The entrainment temperatures T_o^* and T_b^* then can be derived by performing the integrations

$$T_o^* = \frac{1}{\delta}\int_{-h_o-\delta}^{-h_o} SF_T\, dz \tag{49}$$

$$T_b^* = \frac{1}{\delta}\int_{-h_o-h_M}^{-h_o-h_M+\delta} SF_T\, dz \tag{50}$$

As one likely solution which satisfies the conditions mentioned above we suggest a 'double-sine'-distribution for temperature and salinity within the IL as indicated in Fig. 8. Then SF_T is of the form

$$SF_T = \begin{cases} T_2(z) & \text{for } -h_o \geq z \geq -h_o - h_M/2l_{2T} \\ T_3(z) & \text{for } -h_o - h_M + h_M/2l_{3T} \geq z \geq -h_o - h_M \end{cases} \tag{51}$$

where

$$T_2(z) = T_o + (T_M - T_o)\sin\left(-\pi l_{2T}\left(\frac{h_o + z}{h_M}\right)\right) \tag{52}$$

and

$$T_3(z) = T_M + (T_b - T_M)\left[\sin\left(-\pi l_{3T}\left(\frac{h_o + h_M + z}{h_M}\right)\right) + 1\right] \tag{53}$$

Solutions for the structure parameters l_{2T} and l_{3T} can easily be obtained by using (48) and the equation

$$h_M = \frac{h_M}{2l_{2T}} + \frac{h_M}{2l_{3T}} \tag{54}$$

It is obvious that the choice of a different structure function would lead to different results for the entrainment temperatures T_o^* and T_b^*, depending on the vertical temperature gradient within the δ-zone. However, this effect may be compensated for by slightly modifying the thickness of the entrainment zone.

Results of the three-layer model

The ability to improve the calculation of entrainment heat and salt fluxes on the basis of the approach decribed in the chapter above is achieved by introducing an additional parameter, the thickness δ of the entrainment zone. For tidal currents constant with time, however, results equivalent to those of the simple two-layer approach are obtained. The system is characterized by freezing at the ice shelf base because of the heat loss due to molecular heat conduction into the ice. The intermediate layer gains heat and salt from the turbulent bottom layer only during detrainment situations (equation (44)). Steady forcing leads to a balance between production of TKE by shear of the isotropic tidal current at the seafloor and dissipation in the background (equation (40)). Therefore detrainment situations will not take place and there is no interaction between bottom boundary layer and IL. Consequently the IL plays the role of the heat and salt-reservoir for the upper ML. The behaviour of the upper boundary layer is independent of the structure of the ocean below. The two-layer model is therefore adequate if steady forcing is prescribed.

However, the three-layer system is characterized by alternating entrainment and detrainment if unsteady forcing is present. This is valid for both the upper and lower ML. In general the cyclic state of the upper ML is comparable with the behaviour described for the two-layer model. But in comparison to the two-layer approach the rate of ablation $\bar{w}_i$ is considerably reduced (Fig. 9). This result is directly connected to the behaviour of the lower boundary layer during a tidal cycle. In contrast to the upper layer which is

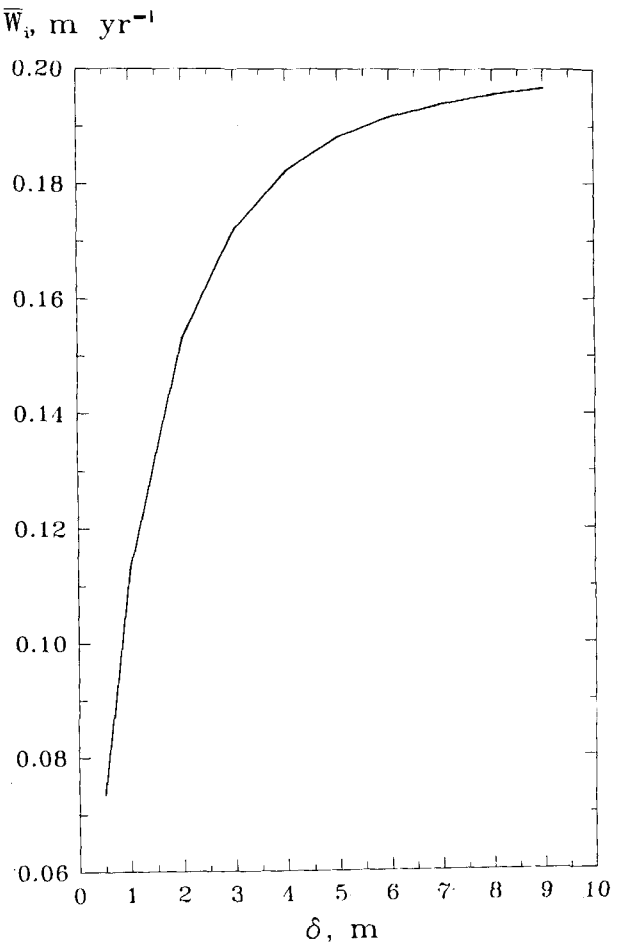


Fig. 9. Dependence of mean melting rate $\bar{w}_i$ on thickness δ of the entrainment zone.

https://doi.org/10.1017/S0954102090000049 Published online by Cambridge University Press

characterized by a high variability (Fig. 4) the lower ML shows only weak fluctuations. The cycle is determined by a weak but prolonging entrainment situation and thus by a very short detrainment period (less than 5% of the cycle time). As stated above the upward heat and salt flux into the IL is restricted to these periods. The 'detrainment-fluxes' into the IL have to be very intensive in order to compensate the heat and salt loss due to the strong entrainment at the top of the IL. This can be realized by establishing high differences of temperature ($T_b^* - T_b$) and salinity ($S_b^* - S_b$). During the entrainment period the development of the lower ML is delayed (equation (40)) because the low-density water of the IL has to be mixed down. However, this effect cannot change the state of the system from entrainment to detrainment.

Detrainment arises when the forcing of the system is nearly at a minimum. In this case production of TKE due to shear of the anisotropic tidal current is balanced by dissipation in the background. The higher the thickness δ of the entrainment zone the higher are the resulting entrainment fluxes at the base of the upper ML and the corresponding melting rates (Fig. 9). The gradient of $\bar{w}_i$ decreases for increasing δ because the vertical gradients of T and S within the IL are decreasing with increasing distance from the discontinuities. The net vertical heat flux amounts to at most 2.0 W m^{-2} if δ = 10.0 m. As indicated above in this case the differences of T and S at the base of the IL have to increase in order to compensate the heat loss of 2.0 W m^{-2} at the top of the IL. This can be realized by a reduction of the mean temperature T_M but this reduction is restricted to the lower temperature T_o of the upper ML. In order to achieve the conservation of heat in the IL the thickness of the upper part of the IL has to increase (Fig. 10). For the maximum thickness of the entrainment zone the ratio of the parameters determining the shape of the 'double-sine'-profile decreases to $l_{2T}/l_{3T} = 0.16$. Thus, the choice of δ modifies the resulting melting rate as well as the structure of the temperature and salinity profiles within the IL. This is an important result which has to be taken into account when calculating the net vertical heat fluxes beneath the RIS especially at station J9.

The model results for the hydrographic structure at station J9 in the central RIS are listed in Table I. On the basis of the current measurements carried out by Jacobs *et al.* (1979) the major axis of the current tidal ellipse is taken to be $U_o = 0.17$ m s^{-1}. The best fit to the conditions beneath the J9-bore-hole is achieved by assuming the minor axis of the tidal ellipse to have the magnitude $V_o = 0.09$ m s^{-1}.

Temperature T_b and salinity S_b of the lower ML are in good agreement with measurements (Jacobs *et al.* 1979) when a time constant $L_\infty/u_a = 2.0 \times 10^6$ s is used for the advection process in the lower boundary layer. According to the advection velocity $u_a = 0.01$ m s^{-1} estimated from MacAyeal (1984*a*) this leads to a length scale $L_\infty = 20$ km. However, the distance of the origin of the HSSW on the western Ross Sea continental shelf amounts to approximately 500 km. This implies that HSSW does not mix with overlying layers on its way to the south until reaching regions where the thickness of the water column is less than approximately 300 m. This is consistent with findings of MacAyeal (1984*a*, *b*) who expected that vertical mixing in the western part of the RIS is suppressed because the tidal energy dissipation is too

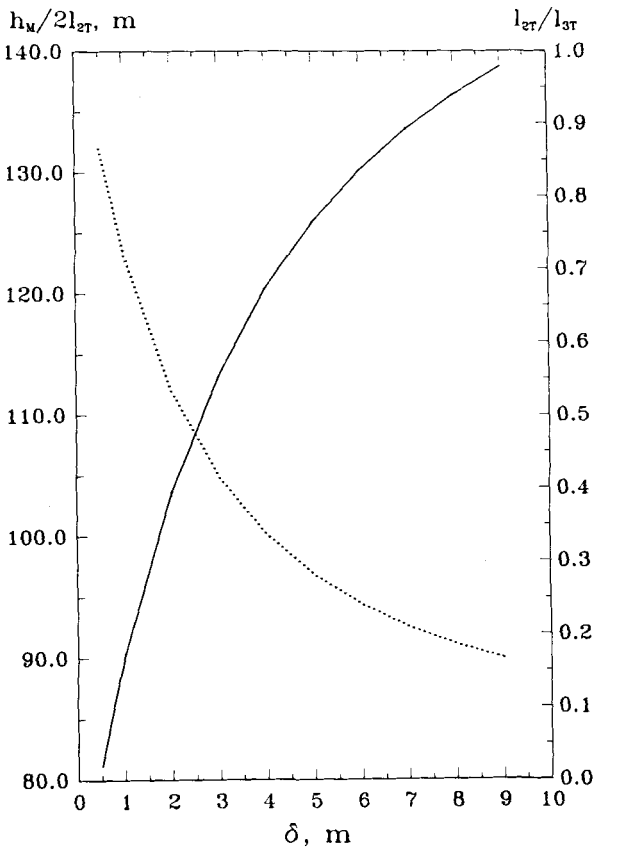


Fig. 10. Thickness $h_M/2l_{2T}$ of the upper part of the intermediate layer and the ratio l_{2T}/l_{3T} of the two sublayers depending on thickness δ of the entrainment zone. $l_{2T}/l_{3T} = 1$ means that the two parts have the same thickness. The mean thickness of the intermediate layer for the present calculations is h_M = 189.0 m. The dashed curve belongs to the ordinate on the right hand side.

Table I. Results of the three-layer model in comparison to observations at station J9. The parameters used are: $U_o = 0.17$ m s^{-1}, $V_o = 0.09$ m s^{-1}, $D_o = 6$, $h_s = 10$ m, $h_c = 50$ m, $\gamma_T = 1.0 \times 10^{-4}$ m s^{-1}, δ = 3 m (p = 363 dbar at the ice shelf base).

Variable	Observation	Simulation
T_1, °C	−2.16	−2.160
S_1,	34.39	34.386
T_o, °C	−2.16 to −2.13	−2.156
S_o,	34.40	34.720
h_o, m	30 to 35	30.8 to 41.5
T_M, °C	−2.05 to −2.06	−2.069
S_M,	34.6	34.752
T_b, °C	−1.86	−1.862
S_b,	34.83	34.832
h_b, m	35 to 40	40 to 42
w_i, m yr^{-1}	−0.03	0.17

https://doi.org/10.1017/S0954102090000049 Published online by Cambridge University Press

weak to destroy the stratification.

The variability of the thickness of the lower ML is very low in spite of the highly anisotropc forcing. The thickness varies between 40 m and 42 m which is in good correspondence with observations (Gilmour 1979). The upper ML shows a high variability with time (30.8–41.5 m). Despite of the lack of measurements to fully describe the behaviour of the upper ML over a tidal cycle, this seems to be a good approximation to real conditions (Foster 1983).

Foster (1983) and Zotikov (1986) stated that the temperature of the layers adjacent to the mixed layers show a very high varability with time. They determined fluctuations up to 0.01°C at the top of the lower boundary layer and up to 0.05°C just below the upper ML. In spite of the extremely anisotropic forcing the model results do not show these high variations over a tidal cycle. This may be due to neglecting the internal wave activity which represents an additional mechanism for dissipation of tidal energy beneath the ice shelf (Foster 1973).

The overestimation of the mean salinity S_o in the upper ML indicates that the advection process in the upper boundary layer missing in the model has strong impact on the hydrographic situation. In order to explain the measured salinity $S_o = 34.40‰$ there is need of advection of less saline melt-water plumes from the deeper reaches of the sub-ice-shelf cavity as proposed by MacAyeal (1984*a*, 1985*b*)

The net vertical heat flux amounts to 1.8 W m^{-2} which corresponds to a mean basal melting rate of 0.17 m yr^{-1}. Disregarding the effect of advection of freshwater produced in deeper regions of the ice shelf the calculated rate of melting can be regarded as the upper limit which may arise if only vertical processes are considered. Based on an ice-core measurement Zotikov (1980) indicated that the ice at station J9 consists of two layers. The upper 410 m of the ice shelf represents fresh ice and the lower 6 m consists of sea ice having salinities from 2‰ to 4‰. Due to the distance of the J9-borehole from the grounding line of the RIS (≈ 200 km) and considering the ice-flow velocities (300–400 m yr^{-1}) the ice at station J9 has been in contact with the ocean for 400 to 600 years. Thus, Zotikov (1986) concluded that the accumulation rate amounts to 1.0–1.3 cm yr^{-1}. However, this is only valid if vertical as well as horizontal heat fluxes are absent in the deeper reaches of the sub-ice-shelf cavity. As shown above this low accumulation rate is correlated to the existence of isotropic tidal currents. Measurements of Jacobs *et al.* (1979) and numerical simulations of MacAyeal (1984*b*), however, indicate a high anisotropy of the current system especially in the immediate J9-area. Therefore the sea ice at station J9 must result from advection of freshwater produced to the south of J9. Because of its low density the melt-water plume rises up into regions of lower pressure. Freezing may occur if the entrainment driven vertical heat flux is not sufficient to hinder the plume to achieve its *in situ* freezing temperature on its way to the north. That accumulation actually may take place if melt-water rises along the sloping ice shelf base was shown by Hellmer & Olbers (1989) on the basis of a two-dimensional circulation model under an idealized ice shelf. MacAyeal (1984*a*) stated that net ablation due to tidal stirring is restricted to the south-eastern part of the RIS where the ice shelf draft exceeds 400 m — the upper limit of the DISW on the Ross Sea continental shelf (Jacobs *et al.* 1985). Station J9 is located approximately 50 km away from this 'boundary'. If advection of freshwater from the south is sufficient to compensate vertical heat and salt fluxes due to the entrainment processes freezing will take place at the ice shelf base. Considering the advection velocity of the ice shelf in the immediate J9-area (300–400 m yr^{-1}) accumulation rates of 0.03–0.05 m yr^{-1} would be necessary to produce a 6 m thick saline ice layer. This estimate is consistent with the accumulation rate of 0.03 m yr^{-1} observed by Zotikov (1986).

Melting and freezing rates are calculated at several locations in the south-eastern part of the RIS based on simulations of the tidal current ellipse of the K_1-tide beneath the RIS carried out by MacAyeal (1984*b*). Selected locations are shown in Fig. 11 and results are listed in Table II. The timescale of the advection process in the lower boundary layer is determined by a length scale L_∞ and the advection velocity taken to be u_a = 0.01 m s^{-1}. The length scale L_∞ may be estimated when considering the expected large scale flow pattern of the HSSW beneath the RIS (see MacAyeal 1984*a*, fig. 4) and assuming that the characteristics of HSSW remain unchanged on its way to the south until the thickness of the water column

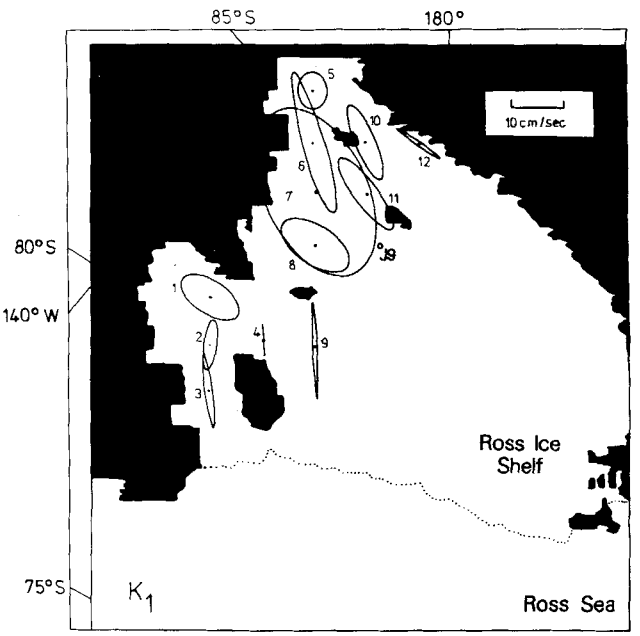


Fig. 11. *Simulated K_1 tidal current ellipses in the south-eastern part of RIS (from MacAyeal 1984a) which are used to determine the local ablation and accumulation rates. The results corresponding to numbered locations are listed in Table II.*

https://doi.org/10.1017/S0954102090000049 Published online by Cambridge University Press

Table II. Model-results at several locations beneath the RIS. Melting rates in brackes indicate the results for half and twice the standard timescale of the advection process within the bottom boundary layer.

Location	U_o; V_o, cm s^{-1}	w_i, m yr^{-1}	
1	6.5; 3.0	0.10	(0.18, 0.06)
2	6.0; 1.0	0.07	(0.11, 0.03)
3	8.0; 0.5	0.04	(0.09, 0.02)
4	4.0; 0.3	0.07	(0.13, 0.04)
5	3.5; 3.0	–0.012	(–0.012,–0.012)
6	14.5; 2.0	0.21	(0.37, 0.11)
7	17.5; 9.5	0.18	(0.19, 0.15)
8	7.5; 4.0	0.16	(0.18, 0.11)
9	9.0; 1.0	0.15	(0.25, 0.08)
10	8.0; 2.0	0.20	(0.32, 0.12)
11	9.0; 2.0	0.27	(0.44, 0.15)
12	6.0; 1.0	0.44	(0.51, 0.35)

becomes less than approximately 300 m. However, this is a somewhat crude estimate so that the calculations were repeated with half and twice that time scales.

Ablation rates exceeding 0.4 m yr^{-1} were obtained, especially to the south-east of Crary Ice Rise where the ablation rates are highest. This region is characterized by a distinct anisotropy of the tidal current ellipse and a thin water column. The results are consistent with an estimate of the net melting rate valid for the considered region. MacAyeal (1984*a*) obtained $w_i = 0.5 \pm 0.25$ m yr^{-1} based on the residence time of HSSW below the ice shelf.

Noticeable are the results at location No. 5 nearest to the grounding line where the tidal current ellipse is nearly isotropic. Accumulation takes place at the ice shelf base independently on the advection time scale. This behaviour emphasizes the influence of the time-variability of the tidal currents on vertical heat and salt fluxes. It turns out that a modification of the advection velocity and/or the length scale result in a different melting rate only if the tidal currents show a distinct anisotropy.

In addition the ablation rate is highly correlated to the thickness of the water column as indicated by MacAyeal (1984*a*). The thinner the water column the higher the gradients of temperature and salinity at the top and at the bottom of the intermediate layer. Consequently entrainment fluxes and the corresponding melting rates increase.

Conclusions

In the first part of this work an integrated mixed layer model which is thermodynamically coupled to the ice shelf was studied. The model consists of a two-layered ocean: a turbulent boundary layer directly beneath the ice shelf and a laminar bottom layer representing an infinite heat and salt reservoir. With the help of this simple approach it is possible to simulate ablation as well as accumulation scenarios at the ice shelf base. The occurrence of melting or freezing depends strongly on the character of the tidal current which is the source of the mechanical energy necessary to lift up the dense water of the bottom layer. The natural assumption that a strong tidal current and the corresponding high production rate of TKE leads to a high ablation rate is only partially true. Of primary importance is the degree of the time-variability of the tidal forcing. If time-independent forcing is prescribed the result is an accumulation rate of 1.3 cm yr^{-1}. In this special case the rate of freezing is determined by the heat loss of the ML into the ice shelf due to molecular heat conduction and is not effected by modifying the model parameters.

Otherwise, if the eccentricity of the tidal current ellipse becomes very large, the rate of melting exceeds 1.0 m yr^{-1}. The model achieves a cyclic state which is characterized by alternating entrainment and detrainment situations. The model reacts most sensitively to the parameterization of the turbulent fluxes at the top of the ML which are assumed to be proportional to characteristic velocities γ_T and γ_S. However, at this stage it is not possible to decide whether the estimates for γ_T and γ_S used for standard calculations lead to realistic ablation rates or not because temperature and salinity of the bottom layer were held fixed. This leads to an overestimation of the upward directed entrainment fluxes and consequently to unrealistic high ablation rates.

Thus, in regard to a local application of the one-dimensional model to the hydrographic conditions beneath the RIS, an extended model was developed. The bottom layer is now treated as a turbulent boundary layer as well and advection of heat and salt is included. Within an additional intermediate layer profiles for T and S are prescribed which comply with the conservation of heat and salt content of this layer. This approach improves the estimate of the entrainment fluxes by mixing the vertical averaged characteristics of an entrainment zone of thickness δ into the turbulent boundary layers.

The model yields good agreement with observations of the hydrographic situation at station J9 in the central Ross Ice Shelf; in particular the thicknesses of the boundary layers as well as their behaviour over a tidal cycle is well reproduced. However, the values assumed for the parameter D_o and the dissipation length scale h_s must be proved, e.g. with the help of dissipation measurements beneath the ice shelf. However, a modified combination of D_o and h_s in order to fit the observed ML-thicknesses is expected to have no significant influence on the resulting ablation rate because the time-variability over a tidal cycle remains nearly unchanged.

In order to fit the temperature distribution below station J9 the characteristic velocity is taken to be $\gamma_T = 1.0 \times 10^{-4}$ m s^{-1} which corresponds to a thickness of a thermal sublayer of 1.3 mm. No agreement was achieved regarding the fluctuations of T and S with time scales less than the tidal period within the layers directly connected to the turbulent boundary layers. This result suggests that the effects of the internal wave field should be considered in further modelling work.

The attempt to fit the salinity within the upper boundary layer failed because advection of freshwater in the upper ML

https://doi.org/10.1017/S0954102090000049 Published online by Cambridge University Press

was disregarded. Based on glaciological data an accumulation rate of 0.03–0.05 m yr^{-1} is expected at station J9 due to the advection of melt-water plumes originating south of J9 though the tidal stirring induces a vertical heat flux of approximately 1.8 W m^{-2}. Therefore melting rates obtained by application of the three-layer model at several locations beneath the south-eastern RIS should be regarded as the maximum amount which could be expected if vertical processes are considered solely. In this case the ablation rates exceed values of 0.4 m yr^{-1} and are correlated to the time-variability of the tidal current, the advection time scale in the lower boundary layer and to the thickness of the water column. Due to the lack of hydrographic data within the considered region of the RIS it is not possible to include the advection process in the upper ML in a reasonable manner. Nevertheless, if improved sets of observations will be available the model presented may be an effective tool to predict local ablation and accumulation rates beneath the ice shelf.

References

Clough, J.W. & Hansen, B.L. 1979. The Ross Ice Shelf Project. *Science*, **203**, 433–434.

Foster, T.D. 1978. Temperature and salinity field beneath the Ross Ice Shelf. *Antarctic Journal of the United States*, **13** (4), 81–82.

Foster, T.D. 1983. The temperature and salinity finestructure of the ocean under the Ross Ice Shelf, *Journal of Geophysical Research*, **88** (C4), 2556–2564.

Gill, A.E. 1973. Circulation and bottom water production in the Weddell Sea. *Deep-Sea Research*, **20**, 111–140.

Gill, A. E. 1982. Atmosphere-Ocean Dynamics. *International Geophysical Series*, **30**. New York: Academic Press, 662 pp.

Gilmour, A. E. 1979. Ross Ice Shelf Sea temperatures. *Science*, **203**, 438–439.

Hellmer, H.H. & Olbers, D.J. 1989. A two-dimensional model for the thermohaline circulation under an ice shelf. *Antarctic Science*, **1**, 325–336

Holman, J.P. 1986. *Heat Transfer*, 6th edition, New York: McGraw-Hill Book Company, 676 pp.

Jacobs, S.S., Amos, A.F. & Bruchhausen, P.M. 1970. Ross Sea oceanography and Antarctic bottom water formation. *Deep-Sea Research*, **17**, 935–962.

Jacobs, S.S., Fairbanks, R.G. & Horibe, Y. 1985. Origin and evolution of water masses near the antarctic continental margin: Evidence from $H_2{}^{18}O/H_2{}^{16}O$ ratios in sea-water, *Antarctic Research Series*, **43**, 59–85.

Jacobs, S.S., Gordon, A.L. & Ardai, J.L. 1979. Circulation and melting beneath the Ross Ice Shelf. *Science*, **203**, 439–443.

Kraus, E.B. & Turner, J.S. 1967. A one-dimensional model of the seasonal thermocline. *Tellus*, **19**, 98–105.

Lemke, P.A. 1987. A coupled one-dimensional sea ice–ocean model. *Journal of Geophysical Research*, **92** (C12), 13164–13172.

Lemke, P. & Manley, T.O. 1984. The seasonal variation of the mixed layer and the pycnocline under polar sea ice. *Journal of Geophysical Research*, **89** (C4), 6494–6504.

MacAyeal, D.R. 1984*a*. Thermohaline circulation below the Ross Ice Shelf: A consequence of tidally induced vertical mixing and basal melting. *Journal of Geophysical Research*, **89** (C1), 597–606.

MacAyeal, D.R. 1984*b*. Numerical simulations of the Ross Sea tides. *Journal of Geophysical Research*, **89** (C1), 607–615.

MacAyeal, D.R. 1985*a*. Tidal rectification below the Ross Ice Shelf. *Antarctic Research Series*, **43**, 109–132.

MacAyeal, D.R. 1985*b*. Evolution of tidally triggered meltwater plumes below ice shelves. *Antarctic Research Series*, **43**, 133–143.

McPhee, M.G., Maykut, G.A. & Morison, J.H. 1987. Dynamics and thermodynamics of the ice/upper ocean system in the Marginal Ice Zone of the Greenland Sea. *Journal of Geophysical Research*, **92** (C7), 7017–7031.

Michel, R.L., Linick, T.W. & Williams, P.M. 1979. Tritium and Carbon-14 distribution in seawater from under the Ross Ice Shelf Project ice hole, *Science*, **203**, 445–446.

Niiler, P.P. & Kraus, E.B. 1977. One-dimensional models of the upper ocean. *In* Kraus, E.B., *ed. The modelling and prediction of the upper layers of the ocean*. Oxford: Pergamon Press, 143–172.

Phillips, O.M. 1977. Entrainment. *In* Kraus, E.B., *ed. The modelling and prediction of the upper layers of the ocean*. Oxford: Pergamon Press, 92–101.

Schlichting, H. 1982. *Boundary layer theory*. [Grenzschicht-Theorie.] 8th edition. Karlsruhe: Wissenschaftliche Bücherei, Verlag G. Braun, 843 pp.

Zotikov, I.A. 1986. *The thermophysics of glaciers*. Dordrecht/Boston/Lancaster/Tokyo: Reidel Publishing Company, 275 pp.

Zotikov, I.A., Zagorodnov, V.S. & Raikovsky, J.V. 1980. Core drilling through the Ross Ice Shelf (Antarctica) confirmed basal freezing. *Science*, **207**, 1463–1465.

https://doi.org/10.1017/S0954102090000049 Published online by Cambridge University Press